A Gas Tension Device for the Mesopelagic Zone

Andrew Reed[a,b,*], Craig McNeil[a,b], Eric D'Asaro[a,b], Mark Altabet[c], Annie Bourbonnais[c], and Bruce Johnson[d]

[a]School of Oceanography, University of Washington, 1503 NE Boat Street, Box 357940, Seattle, WA 98195, USA
[b]Applied Physics Laboratory, University of Washington, 1013 NE 40th Street, Seattle, WA 98105, USA
[c]School for Marine Science and Technology, University of Massachusetts Dartmouth, 706 Rodney French Blvd, New Bedford, MA 02744, USA
[d]Department of Oceanography, Dalhousie University Faculty of Science, 1355 Oxford Street, Halifax, Nova Scotia, Canada B3H 4R2

*Corresponding Author: Andrew Reed, AIRS, Applied Physics Laboratory, University of Washington, 1013 NE 40th Street, Seattle, WA 98105, USA. Email: reedan@uw.edu

Abstract

Gas Tension Devices (GTDs) are used to acquire accurate and stable measurements of gas tension, or total dissolved air pressure of the gases dissolved in water. GTDs operate by measuring the barometric pressure of a small sample volume of air separated from the water by a gas-permeable membrane resting on a rigid permeable support. Existing GTDs use a compressible polydimethylsiloxane (PDMS) membrane which exhibit several undesirable features: the membrane collapses with increasing hydrostatic pressure, which reduces the permeability; a collapsed membrane increases the response; collapse and expansion generate large transient signals [McNeil et al 2006a]. Also, reverse osmosis becomes a problem at depths greater than approximately 330 m in seawater. We present a new GTD that solves the hydrostatic pressure-generated transients and changing response times, and alleviates reverse-osmosis. These improvements allow the new GTD to be used in the mesopelagic zone. The new GTD uses a custom designed small diameter (4 cm) thin (130 µm) incompressible composite Teflon-AF 2400 membrane. It can operate to a depth of at least 1000 m with a depth-independent response time of approximately 35 minutes. We estimated the hydrostatic pressure dependence of Henry's Law solubilities as we characterized the new Teflon-membrane GTD using data collected in the laboratory. Field testing occurred on two APL/UW Gas-Profiling Floats deployed in the Eastern Tropical North Pacific (ETNP) for 15 days during May 2014. The floats profiled between the surface and 400 m depth, sampling gas tension within the Oxygen Deficient Zone. The gas tension-profiles from the two GTDs were validated against gas tension derived from independent N_2:Ar and Ar concentrations measured by mass spectrometry, agreeing to within ±0.6% and ±0.4%.

Keywords: Gas Tension Device, Nitrogen, Dissolved Gas measurements

1. Introduction

Measurements of dissolved gases are widely used in oceanography, limnology, and aquaculture, with dissolved O_2 being the third most frequently measured property of seawater after temperature and salinity. Dissolved gas measurements have been used to study: ocean carbon uptake and acidification [Takahashi et al. 1997]; bubble mediated air-sea gas exchange [Emerson & Bushinsky 2016]; biological production and net community metabolism [McNeil et al. 2006b]; water quality for juvenile hatchery fish downstream of dam spillways [Bragg & Johnston 2016]; denitrification/anammox in anoxic natural and waste waters [Löffler et al. 2011]; and groundwater recharge and trapped gas phases [Manning et al. 2003]. The four major atmospheric components, namely nitrogen (N_2), oxygen (O_2), argon (Ar), and carbon-dioxide (CO_2), are most easily measured using conventional techniques thanks to their large dissolved concentrations and partial pressures. Since they are important to numerous biological and chemical processes, and noting the widespread use of these measurements, there is a continued need to improve dissolved gas sensor measurement technology to overcome current limitations, such as depth dependence, response time, calibration stability, interferences, cost, cross-sensitivity, and power consumption, and improve basic performance characteristics, such as accuracy and resolution.

Of these four gases, dissolved CO_2 and O_2 are the most chemically reactive. Dissolved aqueous CO_2 is normally measured using a nondispersive infrared sensor (NDIR) [Hales et al. 2004]. Dissolved O_2 is measured most accurately using discrete water samples analyzed by the Winkler titration method [Langdon 2010]. Several commercially-available in-situ sensors based on polarographic or fluorescence quenching methods are also used for O_2. Less-reactive dissolved N_2:Ar are measured by mass spectrometry (MS) or gas chromatography [Groffman et

77 al. 2006]. All techniques that require collection, storage, transport, and subsequently analysis of
78 discrete water samples are subject to numerous opportunities for contamination or alteration of
79 the water samples. An in-situ sampling method for measuring dissolved N_2 will help address
80 most of these issues.

81 A gas tension device (GTD) measures the gas tension which is subsequently used to
82 derive in-situ dissolved N_2 if dissolved O_2 is also measured [McNeil et al. 1995]. The first in-situ
83 dissolved gas measurements made using the tensiometer from D'Aoust et al. [1975] and the
84 Weiss saturometer, had accuracies of 3% [Fickeisen et al. 1975]. Gas tension is the total pressure
85 of dissolved gases in a parcel of water. In a GTD, a semipermeable membrane is used to
86 equilibrate a small volume of gas trapped behind the membrane with the gases dissolved in the
87 surrounding water. When the GTD's gas volume is equilibrated with the seawater sample, a
88 barometer in the GTD measures gas tension. Using concurrent measurements of gas tension,
89 dissolved O_2, temperature and salinity, and measured or assumed saturation levels for Ar and
90 pCO_2, dissolved N_2 can also be determined to a final accuracy of ±0.7% [McNeil et al. 1995;
91 McNeil et al. 2005].

92 A custom GTD was designed and used on profiling floats [McNeil et al. 2006a] to
93 measure the rapid changes in gas tension in the ocean mixed layer during the passage of a
94 hurricane [D'Asaro & McNeil 2007]. That GTD used a tubular polydimethylsiloxane (PDMS)
95 membrane with a large surface area and low-internal volume to achieve a response time of
96 minutes. The compressibility of PDMS resulted in two major complications with this GTD. First,
97 the membrane's permeability decreased with increased hydrostatic pressure which resulted in a
98 significantly slower response at increased depths and a hysteresis in the gas tension profiles.
99 Second, the release (uptake) of gases from the membrane during compression (decompression)

resulted in large transient positive (negative) pressure fluctuations in the raw GTD measurements. Another more severe problem was sporadic clogging of the membrane, likely caused by reverse osmosis of liquid water through the membrane into the barometer. These limitations excluded GTD-equipped floats from deep (below 60 meters) or extended deployment and increased measurement error.

This paper describes a new GTD designed to overcome these limitations. Our motivation is to measure dissolved N_2 on profiling floats deeper in the ocean and specifically in oxygen deficient zones (ODZs) to study the biological production of N_2 via the denitrification and anammox processes. We expect a N_2-excess signal of 10 – 20 mbar out of a background 850 mbar based on the N-excess from Chang et al. [2012]. We begin by presenting the design of the new GTD and describing the new materials involved. Next, we lay out the background theory of gas tension measurements, which is used to construct a model which describes the temperature and hydrostatic pressure dependencies. The GTD is then characterized in the laboratory using the developed model, followed by testing in the Puget Sound, and finally deployment in the Eastern Tropical North Pacific (ETNP) ODZ. Then, we present the results of the lab experiments and field testing, with the Puget Sound and ETNP results validated against an independent gas tension estimate calculated with concurrent measurements of dissolved O_2 and N_2:Ar ratios determined by mass spectrometry. Lastly, we discuss how the new GTD-design is an improvement over the previous versions, what needs further development, and future field applications.

2. Instrument Design

Autonomous profiling Gas-floats (Applied Physics Lab, University of Washington), which alter their buoyancy to settle at different isopycnals in the water column, offer a platform for frequent sampling of multiple seawater properties through time and space. An ideal float-mounted gas tension device would measure the gas tension with a rapid (seconds) equilibration (response) time, function independently of temperature and hydrostatic pressure, and function reliably for long-periods of time on autonomous platforms. The previous float-mounted GTD utilized a large (1 m length x 3 cm diameter) tubular PDMS membrane to achieve minute response times [McNeil et al. 2006a]. However, the previously discussed issues of the PDMS-membrane meant the GTD required frequent maintenance and limited possible applications [McNeil et al. 2005; McNeil et al. 2006a].

The new GTD design is shown in Figure 1. It has three main components: (1) a pressure housing, (2) a flushed membrane interface, and (3) a seawater pump. The new design is more compact than the previous version, making it easier to mount and protect. The compressible PDMS membrane is replaced with a nearly-incompressible Teflon-AF 2400 membrane (DuPont). This switch of material reduces response times with hydrostatic pressure and the hysteresis, improving performance and accuracy of the instrument.

However, Teflon-AF 2400 is a difficult material to make flat membranes from because it is brittle and thin sheets of it tend to curl. We settled on a 4 cm diameter by 130 µm thick membrane after some experimentation. The membrane is supported on the non-water side by a fine stainless-steel support mesh. The membrane and support mesh are anchored in a membrane-housing manufactured from Delrin. Stainless-steel 1/16” tubing connects the membrane housing to a Paroscientific Digiquartz Pressure transducer (0-30 psia), which has a manufacturer's stated

precision of 0.0001%, accuracy of 0.01%, and drift of a few parts-per-million per year. The pressure transducer and associated electronics are protected in a separate pressure-housing. Barometric pressure and internal temperature of the GTD is recorded by the float.

The water-side face of the membrane is covered with a plenum that is connected to a SBE5T seawater pump. Flushing the membrane significantly reduces the equilibration time by shrinking the boundary-layer that forms along the membrane-seawater interface. The plenum is a plastic cap with the water inlet situated over the membrane and several small outlets, with their total area less than the inlet, spaced radially around the side of the plenum. This directs the water onto the membrane and shears radially, and maintains a slight positive pressure to ensure the membrane is held flat against its support. The pump is controlled by the GTD electronics and operates on three settings: 100% (continuous), 50% (laboratory only), and 10% (pulse) pumping cycles. Pulse mode is preferred to conserve energy and prolong battery life. Continuous mode is activated during surfacing to protect the membrane from possible damage when bubble and temperature-induced supersaturations at the surface may exceed the hydrostatic pressure, causing ballooning and tearing in the membrane. The GTD mounted on the Argo-float is the same as those mounted on the gas-sensing floats, except it is unpumped and the membrane is left uncovered to improve passive flushing.

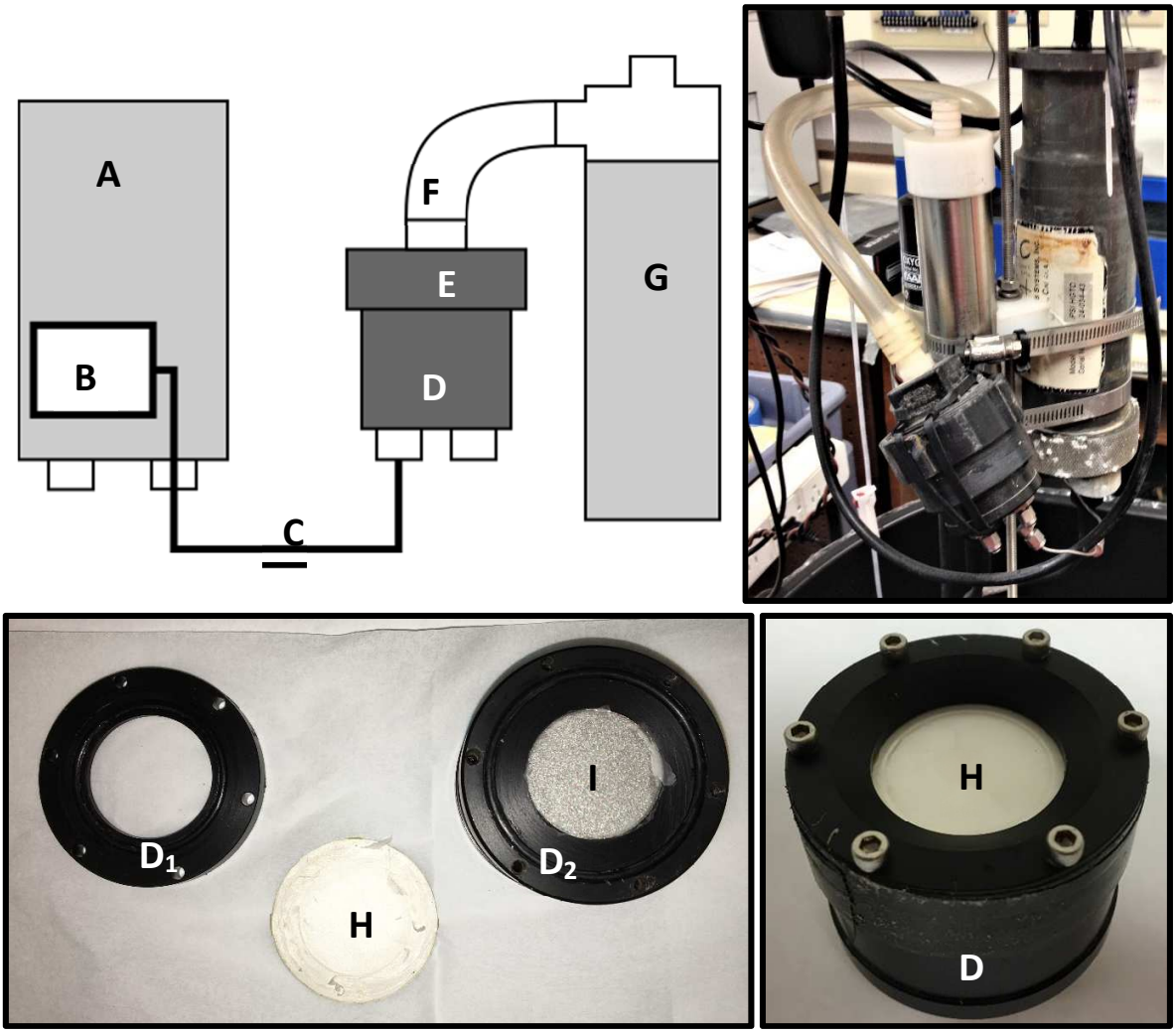

Figure 1. Schematic and pictures of the new GTD, showing clockwise from the top left, the assembled GTD with pump, the disassembled membrane housing, and the membrane housing. A: Pressure housing and electronics, B: Paroscientific barometer, C: 1/16” stainless steel tubing, D: assembled membrane housing (D_1: membrane collar, D_2: main membrane housing), E: plenum, F: plastic tubing, G: Seabird 5T pump, H: Teflon membrane and support, I: Stainless steel mesh support.

3. Methods

3.1. Theory & Modeling

3.1.1. Gas Tension in Seawater

A measurement of gas tension in seawater needs to be corrected for hydrostatic pressure and temperature [Hamme et al. 2015]. This can be seen with the following derivation for the gas tension changes in a parcel of water. Gas tension (*GT*) of seawater is defined as the sum of all the partial pressures (p_i) of the dissolved gases in seawater:

$$GT = \sum_i p_i = p\mathrm{N}_2 + p\mathrm{O}_2 + p\mathrm{Ar} + p\mathrm{H}_2\mathrm{O} + p\mathrm{CO}_2 + p\mathrm{Trace} \qquad \text{Eq. (1)}$$

In the above equation i denotes contributions due to individual gases [McNeil et al. 1995]. We define the total contribution to gas tension of all traces gases (including neon, krypton, nitrous oxide, methane, etc.) with partial pressures less than $p\mathrm{CO}_2$ by $p\mathrm{Trace}$. The relative contribution of each denoted gas to a measurement of gas tension in two different types of seawater are shown in Table 1. For the first water type (Table 1, Column 1a) we chose representative values of the core of the ODZ in the ETNP off Mexico. Since these waters are anoxic, there is no contribution to gas tension by dissolved oxygen. Dissolved nitrogen contributes more than 97.3% of the gas tension, with another 1.3% from water vapor, 1.1% from argon, 0.16% from carbon dioxide, and less than 0.02% from other trace gases. In anoxic ODZ core waters, a small percentage (typically <4% or <30 mbar) of the measured pN_2 is associated with microbial denitrification and anammox of nitrogen containing nutrients. For the second water type (Table 1, Column 2a), we chose surface waters in equilibrium with the atmosphere in the same location. Compared to the ODZ core waters, gas tension in the oxygenated surface water is significantly larger (>15%), and pH_2O increased sharply with increased temperature by approximately a factor of three.

194 The classical Henry's Law is used to relate the partial pressure, p_i, of a dissolved gas in
195 water to the concentration, $[C_i]$, of the dissolved gas by:

$$p_i = \frac{[C_i]}{Sol_i(T,S)} \quad \text{Eq. (2)}$$

196 The Henry's Law solubility $Sol_i(T,S)$ for a gas is dependent on water temperature (T) and
197 salinity (S). However, Klots [1961] identified that hydrostatic pressure also influenced
198 Sol_i, which depended on the partial molal volume of the gas in solution. The importance of this
199 effect when utilizing a GTD was identified by Hamme et al. [2015].
200 The GTD makes a measurement of the pressures of all the dissolved gases at equilibrium
201 with the surrounding water. Consequently, we used a modified form of Henry's Law in which
202 the gas partial pressures were replaced with the gas fugacities, which more accurately
203 represented the effective partial pressures of the gases in chemical equilibrium with the effective
204 (i.e. actual) concentrations. Following Ludwig and MacDonald [2005], the effect of hydrostatic
205 pressure on gas fugacities was expressed as:

$$\left(\frac{\partial \ln(f_i)}{\partial P}\right)_{T,C_i} = \frac{V_i}{RT_K} \quad \text{Eq. (3)}$$

206 where f is the fugacity (atm), V_i is the molal volume (ml mol^{-1}), R is the universal gas constant
207 (≈82.057 mL atm mol^{-1} K^{-1}), and (T_K) is the absolute temperature (K). Assuming constant molal
208 volumes and concentrations, integrating between hydrostatic pressures and solving for the
209 fugacity yielded [Ludwig & MacDonald 2005]:

$$f_i(P) = f_i(P_{1\text{ atm}}) \cdot e^{\frac{V_i * \Delta P_H}{RT_K}} \quad \text{Eq. (4)}$$

210 Thus, the in-situ gas fugacity $f_i(P)$ at a particular hydrostatic pressure P is equal to the gas
211 fugacity at the sea surface $f_i(P_{1\text{ atm}})$ scaled by the change in hydrostatic pressure ΔP_H (atm) and
212 the gas molal volume (V_i). Equation 4 predicted an increase in gas tension of approximately 14%

213 per 1000 dbar using partial molal volumes of $N_2 \approx 33.1$ ml mol^{-1}, $O_2 \approx 32.0$ ml mol^{-1}, and Ar ≈
214 32.1 ml mol^{-1} [Hamme et al. 2015]. This agreed with the results from an experiment by Enns et
215 al. [1964].

216 The physical interpretation of Equation 4 is that increased hydrostatic pressure increased
217 the tendency of gas to leave solution, or, equivalently, increased hydrostatic pressure decreased
218 gas solubility (concentrations remain unchanged). We recast Equation 2 to relate the in-situ gas
219 fugacity as a function of dissolved gas concentrations and a hydrostatic pressure dependent gas
220 solubility:

$$f_i(P) = \frac{[C_i]}{Sol_i(T,S,P)} \qquad \text{Eq. (5)}$$

221 The effect of rapidly (i.e. adiabatically and with no change in the dissolved gas
222 concentrations [µM/kg]) altering hydrostatic pressure by 400 dbar on seawater gas tension is
223 shown in Table 1 for representative ODZ core waters (Column 1b), and for air-saturated surface
224 waters (Column 2b). For a surface seawater sample that was initially in equilibrium with the
225 atmosphere and then taken rapidly to 400 dbar, the sample's gas tension will increase by
226 approximately 5.2% due to a decrease in the solubility of the gases. Conversely, bringing a
227 seawater sample from the ODZ core to the sea surface, as occurs during a hydrocast, will cause a
228 decrease in gas tension of approximately 5.4% due to an increase in gas solubilities. Note that in
229 both examples, the effects of changes in temperature (< 0.1 °C) due to adiabatic
230 expansion/contraction on gas solubility are small (5.4% vs 5.2%). Not correcting for the
231 hydrostatic pressure effect will lead to systematic overestimation of in-situ gas tension and,
232 consequently, gas concentrations. The effect of the pump's pressure head is negligible if the
233 hydrostatic pressure is relatively large.

234

	Anoxic ODZ Seawater T=9.6°C, S=34.65			**Atm. Equilibrated Seawater T=28.0°C, S=34.72**		
Column	1a	1b	% Total	2a	2b	% Total
Hydrostatic Pressure	400 dbar	*0 dbar*		0 dbar	*400 dbar*	
Gas Tension	878.9 ±1.2	*831.2 ±1.2**	100	1013.3 ±0.2*	*1066.0 ±3.8*	100
fN$_2$	855.4 ±2.6	*808.7 ±2.6**	97.3	762.3 ±1.1*	*803.5 ±1.2*	75.2
fO$_2$	< 0.1	*< 0.1**	< 0.1	204.5 ±1.0*	*215.2 ±1.1*	20.2
fAr	9.9 ±0.5	*9.4 ±0.5**	1.1	9.1 ±0.5 *	*9.6 ±0.5*	0.9
fCO$_2$	1.4 ±0.2	*1.3 ±0.2**	0.2	0.3 ±0.2*	*0.3 ±0.2*	< 0.1
fTrace	< 0.2	*< 0.2**	< 0.1	< 0.2*	*< 0.2*	< 0.1
fH$_2$O	11.8 ±0.3	*11.7 ±0.3**	1.4	37.1 ±0.3*	*37.4 ±0.3*	3.7

Table 1. Dissolved gas composition of a seawater parcel varies significantly between the oxic and anoxic ocean. The individual partial pressures of dissolved gases with their approximate absolute levels (in mbar) and best error estimates that comprise the gas tension of seawater for anoxic core ODZ (Column 1a) using our measurements at 400 dbar in the ETNP, and for surface seawater in equilibrium with the atmosphere (Column 2a) using observations at the sea surface at the same location. Calculations based on an assumed adiabatic change in hydrostatic pressure of 400 dbar by either raising a sample of the anoxic core to the sea surface (Column 1b) or lowering a sample from the sea surface to 400 dbar depth (Column 2b). Argon is assumed saturated ±5%, which is a maximum likely deviation from equilibrium [Hamme & Emerson 2004]. Oxygen within the ETNP ODZ core was measured on the order of ≈100 nM [Tiano et al. 2014]. CO_2 is taken from the World Ocean Database [Boyer et al. 2013]. Water vapor is assumed to be 100% saturated and calculated as an explicit function of temperature and adjusted for salinity effects [Kennish 1989]. Gas tension values are taken from lab and/or field measurements. *We assume that at the ocean surface the gas fugacities behave as ideal gases such that the fugacity is equal to the gas partial pressures p_i. This means that there is no hydrostatic pressure effect at 0 dbar.

3.1.2. Observing Temporal Changes of Gas Tension

Observations of gas tension are first made in the laboratory using a sealed pressure test vessel to understand how the new GTD responds to rapid in situ changes in hydrostatic pressure at constant temperature and dissolved gas concentrations. In practice, the test vessel slowly warmed as the room changed temperature and the dissolved oxygen concentration inside the test tank decreased due to oxidation (microbial and chemical). We compensated for these relatively small and slow variations in gas tension during analysis. In the field, a Lagrangian float carried

the new GTD which equilibrated to the gas tension of individual parcels of water which the float tracked over time. There are similarities between these two measurement approaches which influenced how we formulated the description of the sensor response below. Our intent is to process both data sets similarly. For both types of data sets, changes in temperature and dissolved gas concentrations in the water parcel or enclosed in the pressure test tank are assumed to vary slowly compared to the response time of the sensor to achieve equilibrium of the GTD. We do not use the GTD in a CTD-like profiling mode.

We start by considering the changes to the gas tension of a single water parcel with time (dGT^{sw}/dt). We decompose the changes into several independent components: those due to the temperature effect on solubility ($\partial GT^{sw}/\partial T$), the hydrostatic pressure effect on solubility ($\partial GT^{sw}/\partial P$), the water vapor partial pressure ($\partial p\mathrm{H_2O}/\partial T$), and any internal sources or sinks (R):

$$\frac{dGT^{sw}}{dt} = \frac{\partial GT^{sw}}{\partial T}\frac{\partial T}{\partial t} + \frac{\partial GT^{sw}}{\partial P}\frac{\partial P}{\partial t} + \frac{\partial (p\mathrm{H_2O})}{\partial T}\frac{\partial T}{\partial t} + Q \qquad \text{Eq. (6)}$$

The superscript *sw* indicates seawater. The temperature and hydrostatic pressure terms are a combination of the individual solubility changes to dissolved N_2, O_2, and Ar, scaled by their respective atmospheric mole fractions. For simplicity we separate the water vapor partial pressure contribution to the gas tension. We ignore the small changes in solubility due to salinity variations.

We linearize the dependencies of Equation 6 with the following substitutions: α (%/°C) for the temperature effect on gas tension, β (%/1000 dbar) for the hydrostatic pressure effect on gas tension, and γ (mbar/°C) for change in water vapor due to temperature, and scale the changes with respect to the initial gas tension of the seawater parcel GT_0^{sw}:

279 $$\alpha \equiv \frac{1}{GT_0^{sw}}\frac{\partial GT^{sw}}{\partial T}, \quad \beta \equiv \frac{1}{GT_0^{sw}}\frac{\partial GT^{sw}}{\partial P}, \quad \gamma \equiv \frac{\partial pH_2O}{\partial T}$$

280 This yielded a simplified linear expression for Equation 6:

$$\frac{dGT^{sw}}{dt} = GT_0^{sw}\left(\alpha\frac{\partial T}{\partial t} + \beta\frac{\partial P}{\partial t}\right) + \gamma\frac{\partial T}{\partial t} + Q \qquad \text{Eq. (7)}$$

281 The above equation described the specific case where the sampled water parcel has no external
282 exchange with the surrounding environment, such as in a laboratory setting.

283 Integrating Equation 7 with respect to time yielded a discrete expression for the water gas
284 tension at time *t* (subscript t) with changes due to temperature, hydrostatic pressure, and biology:

$$GT_t^{sw} = GT_0^{sw} + GT_0^{sw}\big(\alpha(T_t - T_0) + \beta(P_t - P_0)\big) + \gamma(T_t - T_0) + Q(t - t_0) \qquad \text{Eq. (8)}$$

285 Note that Equation 8 describes the actual gas tension in the water parcel, which responds
286 instantaneously to changes in the driving forces *P, T,* and *Q*.

287 Now we discuss the response of the sensor, i.e. the GTD, to the change in gas tension of
288 the water parcel surrounding the sensor. A change in the gas tension of the surrounding water
289 parcel (Equation 6) creates a gas pressure differential across the GTD membrane between the dry
290 and water-facing sides. This difference in pressure equilibrates with a characteristic response
291 time τ. The sensor output (GT_t^{GTD}) is a low-pass filtered (i.e. smoothed) version of the water gas
292 tension (GT_t^{sw}). Note the use of superscripts to differentiate between the gas tension in the water
293 (*sw*) and the output from the GTD (*GTD*). We modeled the change in the GTD output
294 (dGT^{GTD}/dt) as a mathematical convolution operation $(*)$ of the changing seawater gas tension
295 (dGT^{sw}/dt) with the sensor response $\left(\frac{1}{\tau}e^{\frac{-t}{\tau}}\right)$:

$$\frac{dGT^{GTD}}{dt} = \frac{dGT^{sw}}{dt} * \frac{1}{\tau}e^{\frac{-t}{\tau}} \qquad \text{Eq. (9)}$$

296 Importantly, the pressure measured by the barometer in the GTD is not the seawater gas tension
297 until the GTD is fully equilibrated (i.e. $t > 5\tau$). In-situ seawater gas tension is obtained by
298 deconvolving (i.e. reversing the convolution in Equation 9) the measured GTD time series with
299 the sensor response. The response time of the GTD depends on both the flushing of the water-
300 side boundary layer and the gas flux through the membrane, which is temperature dependent.
301 Consequently, the response time for any particular deployment or experiment may vary based on
302 the environment, the geometry of the GTD setup, and available power for pumping or flushing.
303 As a result, we calculate a new optimal response time for each individual deployment or
304 laboratory experiment. However, convolution/deconvolution of a time series requires that the
305 response time be constant for the entire time series. For an analysis of how pumping affects the
306 response of a GTD (not the same as the one analyzed here), please see McNeil et al [2006a].
307 The temperature dependence of the response time is related to the temperature
308 dependence of the membrane permeability. Gas transport across a non-porous polymer, such as
309 Teflon-AF, occurs via a solution-diffusion process. The membrane permeability P_m is a function
310 of the membrane solubility S_m and membrane diffusivity D_m [Pinnau & Toy 1996]:
311

$$P_m = S_m \times D_m \qquad \text{Eq. (10)}$$

312 Previous characterization of Teflon-AF 1600 demonstrated that the permeation rates of light
313 gases, such as N_2, O_2, and CO_2, increased with increasing temperatures and concentrations but
314 were independent of pressure [Alentiev et al. 2002]. Additionally, permeability was inversely
315 related to molecular size [Alentiev et al. 2002; Bernardo et al. 2009]. These properties indicate
316 that permeability of Teflon-AF is diffusion-limited, and hence the temperature dependence (i.e.,

317 $\partial P_m/\partial T$) is primarily controlled by the temperature dependence of D_m rather than S_m
318 (i.e., $S_m \times \partial D_m/\partial T >> D_m \times \partial S_m/\partial T$).

319 Equilibration time for a diffusion-limited process was calculated as a function of the
320 membrane diffusivity (D_m), the membrane thickness (h), surface area (A), and the total sample
321 volume of the GTD (V) using:

$$\tau(T) = \frac{hV}{D_m(T)A} \quad \text{Eq. (11)}$$

322 The thickness, surface area, and volume were constants independent of temperature. Thus, the
323 response time is a function of temperature $\left(\tau(T)\right)$ and will be inversely related to the
324 temperature-induced changes in membrane diffusivity.

325 Diffusion-dominated gas-permeation temperature dependence through Teflon-AF is
326 typically empirically fit using an Arrhenius equation [Pinnau & Toy 1996; Alentiev et al. 2002].
327 We assumed a similar temperature-dependence of the response times:

$$\frac{1}{\tau(T)} = \frac{1}{\tau_0} e^{-\frac{E}{RT}} \quad \text{Eq. (12)}$$

328 The pre-exponential factor τ_0 (s^{-1}) and constant E (kJ mol^{-1}) are calculated from a linear fit to the
329 plot of $\ln(1/\tau)$ against $1/T$ (Arrhenius plot).

330 Teflon-AF is eight-fold more permeable to water vapor than nitrogen [Bernardo et al.
331 2009]. Thus, we calculated the water vapor contribution as an instantaneous signal. Gas tension
332 with the water vapor subtracted is referred to as dry gas tension. Substituting Equation 7 into
333 Equation 9 and integrating with respect to time yielded an analytical solution of the GTD
334 behavior to a change in the gas tension of the water parcel:

$$GT_t^{GTD} = GT_0^{GTD} + \left(GT_0^{sw}\left(\alpha(T_t - T_0) + \beta(P_t - P_0)\right) + Q(t - t_0)\right) * \frac{1}{\tau} e^{\frac{-t}{\tau}} + \gamma(T_t - T_0) \quad \text{Eq. (13)}$$

335

3.1.3. Modeling Gas Tension

We adapted Equation 13 by letting $GT_t^{GTD} = GT_t^{Model}$. We also assume that the GTD starts out in both thermal and gas tension equilibrium with the surrounding seawater, so that $GT_0^{GTD} = GT_0^{sw}$. The result is a step-response model that predicted the gas tension recorded by the GTD at time *t*. This model was applied to derive the best fits for the parameters α, β, τ, and Q, which were calculated using a global unconstrained minimization routine [Lagarias et al. 1998]. The algorithm trained the best-fit parameter values by minimizing the MSE between the measured time series (GT_t^{GTD}) and the model of the GTD $\left(GT_t^{Model}\right)$:

$$(\alpha, \beta, \tau, Q)_{mmse} = \min\left[\frac{1}{n}\sum_{t=1}^{n}\left(GT_t^{GTD} - GT_t^{Model}\right)^2\right] \quad \text{Eq. (14)}$$

Using the best fit α, β, and Q, we can calculate a normalized gas tension (GT^{norm}) time series by removing the effects of temperature, hydrostatic pressure, biology, and water vapor:

$$GT_t^{norm} = GT_t^{GTD} - GT_0^{GTD}\alpha(T_t - T_0) - GT_0^{GTD}\beta(P_t - P_0) - Q(t - t_0) - \gamma(T_t - T_0) \quad \text{Eq. (15)}$$

Applying Equation 15 yielded an idealized isothermal, isobaric model of constant gas tension with an explicit solution for an individual re-equilibration:

$$GT_t^{Model} = GT_0^{norm} + (GT_0^{sw} - GT_0^{norm})e^{-\frac{t}{\tau}} \quad \text{Eq. (16)}$$

An example is shown in Figure 3. This idealized model allowed an independent check of the response time of the sensor by a regression fit of the data from the experiment to Equation 16. The result was multiple estimates of τ at different hydrostatic pressures to determine the pressure dependence of τ.

In addition to changing gas levels, profiling between surface and depth may also create a difference between the internal GTD temperature (T^{GTD}) and surrounding water temperature as

354 measured by the float CTD (T^{CTD}). This difference exists because the barometer and the
355 electronics pressure housing contain significant mass, much of which is not in direct contact with
356 the surrounding water (Figure 1). The GTD thermal response time φ described the equilibration
357 of T^{GTD} to T^{CTD}. We constructed a model to fit φ by first quantifying the changes of the GTD
358 temperature with respect to time (dT^{GTD}/dt) as a convolution of the change in temperature
359 measured by float CTD (dT^{GTD}/dt) with a characteristic temperature equilibration $\left(\frac{1}{\varphi}e^{-\frac{t}{\varphi}}\right)$:

$$\frac{dT^{GTD}}{dt} = \frac{dT^{CTD}}{dt} * \frac{1}{\varphi}e^{-\frac{t}{\varphi}} \quad \text{Eq. (17)}$$

360 Equation 17 has an explicit solution of the same form as Equation 16. This resulted in a model of
361 the GTD temperature (T^{Model}) at time *t*:

$$T_t^{Model} = T_0^{CTD} + \left(T_0^{GTD} - T_0^{CTD}\right)e^{-\frac{t}{\varphi}} \quad \text{Eq. (18)}$$

362 The value for φ is calculated in a similar manner to the parameters in Equation 13 by minimizing
363 the MSE between T_t^{GTD} and T_t^{Model} as followed in Equation 14.

364 The thermal response time introduced a lag between the internal GTD temperature (°C)
365 and the surrounding water temperature as measured by the CTD. Starting with the ideal gas law,
366 we relate the disequilibrium ΔT^{Dis} due to the lag between the CTD temperature and the GTD
367 temperature to a disequilibrium ΔGT^{Dis} between the actual gas tension and the GTD reading:

$$\frac{GT_t^{GTD}}{(T_t^{CTD} + 273.15)} = \frac{\left(GT_t^{GTD} + \Delta GT_t^{Dis}\right)}{\left((T_t^{CTD} + 273.15) + \Delta T_t^{Dis}\right)} \quad \text{Eq. (19)}$$

368 This assumes both no net transfer of gas across membrane (constant *n*) and the volume of the
369 GTD remains unchanged (constant *V*). Rearranging, we have an equation describing the gas
370 tension disequilibrium as a function of the temperature disequilibrium:

$$\Delta GT_t^{Dis} = GT_t^{GTD} \frac{\Delta T_t^{Dis}}{(T_t^{CTD} + 273.15)} \quad \text{Eq. (20)}$$

Since the temperature disequilibrium is a transient, its effect on the gas tension is also transient and dependent on the temperature equilibration timescale. So long as $\varphi \leq \tau$, we did not explicitly account for the transient when fitting the GTD observations, because the signal disappeared as the GTD reached gas tension equilibrium with the surrounding water. However, it is important to remain aware of this effect, as the specific configuration of the instrument on a platform may alter the thermal equilibration time.

The time series collected by the GTD required processing to arrive at a sample seawater gas tension. Initially, the water vapor is subtracted from the GTD time series. Then the dry GTD time series is deconvolved with the response time by inverting Equation 9. Next, the deconvolved time series is low-pass filtered. The filtered data is then averaged over each segment of the time series that the GTD was held at the same isopycnal, which we labelled 'drifts'. The result was a single measurement of the dissolved gas tension minus water vapor, referred to as dry gas tension, for each float drift.

3.2. Experimental Methods

3.2.1. Laboratory Methods

GTD performance, design limits, and membrane-properties were assessed in the laboratory with several experiments. In Experiment 1, two GTDs with Teflon-membranes (S/N 43 & 44) were placed in a large pressure test vessel (PTV) filled with freshwater at equilibrium with one standard atmosphere. Over 15 days the hydrostatic pressure was changed in increments of approximately 70 dbar up to a maximum of 300 dbar, with variability of ± 2.5 dbar. Each

isobaric test was maintained for a minimum of 24 hours. Pumping was set at 50% cycle. Temperature, GTD barometric pressure, and hydrostatic pressure were recorded once per minute.

The collected time series were modeled using the model described by Equation 13. The effects of hydrostatic pressure, temperature, respiration on gas tension (via decreasing oxygen), along with the response times, were fit following Equation 14. Parameter standard errors are the diagonal of the covariance matrix (C), which is calculated following the equation $C = \sigma^2(J^TJ)^{-1}$, where J is the Jacobian matrix. With the fitted model parameters, the gas tension time series were normalized following Equation 15. Each equilibration of the GTD, identified by discontinuities in the normalized time series, was fit using the simplified model in Equation 16 to investigate any effect of hydrostatic pressure on the response times of the GTD.

Another experiment assessed the operational hydrostatic pressure range of the Teflon membranes. Two Teflon-membranes and housings were placed in a PTV and the hydrostatic pressure slowly raised to 550 dbar. The membranes were held at 550 dbar for over 24 hours. This was followed by rapid cycling between ambient pressure (60 dbar) and 550 dbar in the PTV. Using a custom-design bulkhead that allowed us access to the dry side of the membrane and housing while the system is pressurized, we tested for presence of water using a syringe to evacuate the volume behind the dry-side of the membrane, which would indicate membrane failure or reverse osmosis.

Separately with Experiment 2, the Teflon-temperature dependence was assessed by measuring the equilibration time of the GTD from 5 – 30°C, a typical range for field measurements. The GTDs were submerged in a containment vessel filled with atmospheric-equilibrated freshwater. The containment vessel is placed within a temperature-controlled water bath. Addition of degassed water (by boiling for > 10 minutes and cooling while sealed from the

415 atmosphere) induced a step-change in the gas tension. Gas tension and temperature were
416 recorded once every 30 seconds. The GTDs equilibrated for a minimum of six e-folding times,
417 and the resulting curves fit to estimate the effect of temperature on response times.
418
419 **3.2.2. Site Descriptions and Field Methods**
420 Initial field-testing in seawater occurred off Shilshole, Seattle, Washington, in the Puget
421 Sound April 16th – 20th 2014 aboard the UW/APL vessel *R/V Robertson*. Two UW/APL Gas
422 Floats #77 and #78 (F77 & F78) were respectively equipped with pumped GTDs #44 and #43
423 (GTD#44 & GTD#43). First, the floats were attached to a stand and lowered by crane to set
424 depths off the side of the ship. This was followed by a series of untethered calibration dives
425 between the surface, 140 dbar, and 70 dbar. Discrete water samples were collected at 5 meter
426 increments bracketing the calibration depths of the GTDs.
427 The two UW/APL Gas-Profiling Floats F77 and F78 equipped with pumped GTDs, along
428 with a prototype un-pumped GTD-equipped Argo float (GTD-Argo), were deployed from the
429 *R/V New Horizon* in the ETNP as part of the *NH1410* research cruise. In May 2014, the floats
430 were deployed approximately 2 kilometers apart at 20.08°N 107.07°W for cross-calibration of
431 the instrumentation, and subsequently drifted northwest over the course of the 15-day
432 deployment.
433 During initial deployment, both floats performed a series of calibration profiles with
434 concurrent CTD casts. Niskin bottles at the calibration pressures were collected for N_2:Ar
435 measurements and Winkler titrations. The float profiles targeted predetermined isopycnals by
436 adjusting their density to be neutrally buoyant. A profile consisted of an initial dive to a max
437 density, followed by a series of drifts at decreasing densities in the water column. Each float drift

lasted 2-3 hours, sufficient time for the GTD to fully equilibrate. Float 77 was recovered during initial deployment due to a malfunction and redeployed for four days at the end of *NH1410*.

3.2.3. Standard Reference Methods

Gas tension measurements by the GTD were validated against a gas tension estimate calculated from independent dissolved gas concentration measurements of N_2, O_2, and Ar. The SeaBird 43 and Anderaa optode dissolved oxygen data were calibrated using in situ Winkler titration measurements. N_2:Ar ratios were measured by the Isotope Biogeochemistry Group (School of Marine Science and Technology, University of Massachusetts-Dartmouth). Puget Sound N_2:Ar and O_2:Ar ratios were measured from discrete bottle samples in the lab at UMass-Dartmouth by Isotope-Ratio Mass Spectrometry [Charoenpong et al. 2014]. ETNP N_2:Ar ratios were sampled at sea via Quadrupole Mass Spectrometry.

ETNP background argon concentrations are provided by Clara Fuchsman, which were collected as an onshore-offshore transect from 18.39°N 104.99°W to 14.00°N 110.00° in the ETNP in 2012 as part of a separate project [Fuchsman et al 2017]. Argon concentrations were measured by isotope dilution [Hamme and Emerson 2004b]. Then, we developed and used a linear-mixing-model based on T-S analysis to interpolate the ETNP 2012 argon concentration data to our observations.

To derive an independent gas tension for validating the GTD in the OMZ, first the measured N_2:Ar ratios were multiplied by the interpolated background argon concentrations to calculate the nitrogen concentrations. Next the nitrogen and argon concentration were converted to partial pressures using Henry's Law including the literature hydrostatic pressure dependence of 14% 1000 $dbar^{-1}$ [Enns et al. 1964; Ludwig & MacDonald 2005]. Water vapor pressure was

explicitly calculated assuming 100% saturation [Kennish 1989]. The pCO_2 was taken from climatology (≈1.4 mbar in the ETNP OMZ) [Boyer et al. 2013]. Typical concentrations of the remaining trace gases contributions fall below the instrument noise level and thus are considered negligible.

4. Results

4.1. Laboratory Characterization

In the laboratory, the two GTDs measured ±0.2 mbar of each other (Figure 2, note the timeseries are purposefully offset for clarity of presentation). Temperature varied between 20 – 22°C. Using Equation 14 best-fit values for τ, α, β, and Q, are shown in Table 2. The modeled time series calculated using Equation 16 and the results in Table 2 compared with the collected time series have standard deviations of 1.87 and 1.25 mbar (≈0.2%) for GTD#43 and GTD#44, respectively (Figure 2).

Applying Equation 15 to normalize the gas tension time series, the response times calculated with Equation 16 range from 26.8 min to 48.8 min (Figure 3) with a mean $\tau \cong 35$ min, independent of hydrostatic pressure. The response times for GTD#43 also increased over time. This compares with $\tau \cong 20$ min calculated using Equation 14. This difference between response times and the individual curve fits are due to the fitting procedure. The model is finding global parameter values that best reproduce the time series, whereas the individual curve fits are optimally-fitting the transient response of the GTD to a large change in gas tension. The best-fit response time for the field deployments was $\tau \cong 36$ min.

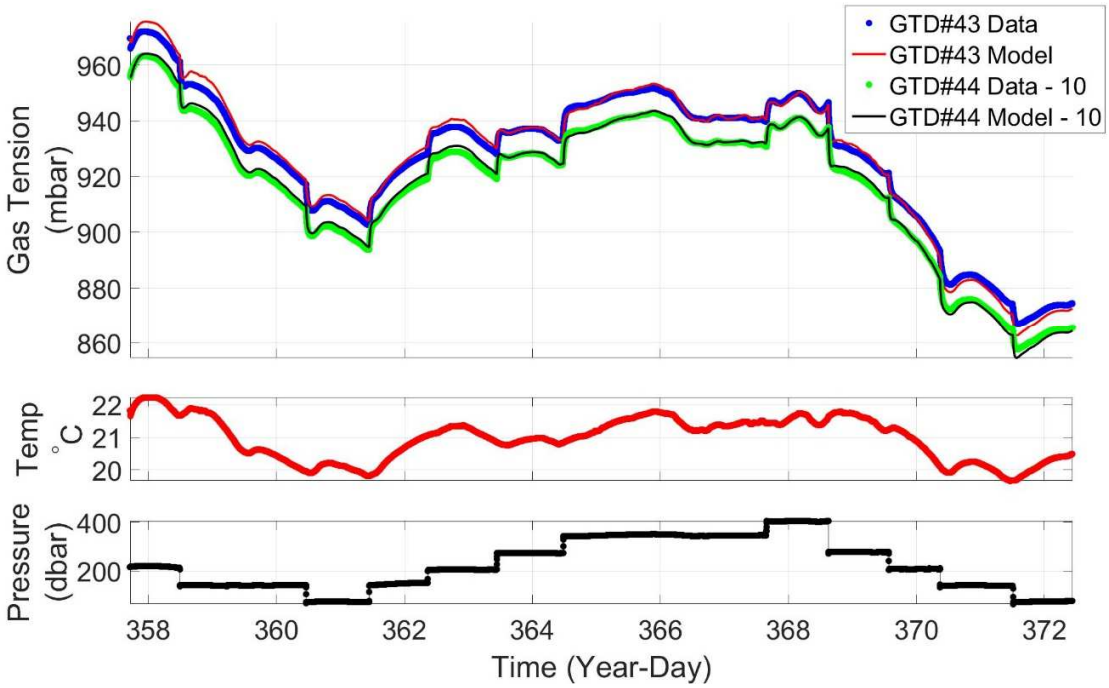

Figure 2. Results of lab experiment 1 - The model described by Equation 13 successfully recreates the observed gas tension time series to within ±1.87 (GTD#43) and ±1.25 mbar (GTD#44) using the best fit parameters (Table 2) calculated following Equation 14. Note the GTD#44 data and model is offset by 10 mbar for both time series to be visible.

Parameter ± SE	**GTD#43**	**GTD#44**
τ (min)	21.36 ± 0.30	20.22 ± 0.34
α (%/°C)	1.67 ± 0.03	1.63 ± 0.02
β (%/1000 dbar)	12.78 ± 0.2	12.98 ± 0.14
Q (mbar/min)	$-2.70*10^{-3} \pm 2.31*10^{-6}$	$-2.60*10^{-3} \pm 1.41*10^{-6}$
GT σ (mbar)	± 1.87	± 1.25

Table 2. Lab experiment 1 - Model parameter best-fit values and standard errors trained on the laboratory gas tension time series from the first laboratory experiment. Data collected with 50% pumping. Response time τ is assumed independent of hydrostatic pressure and temperature.

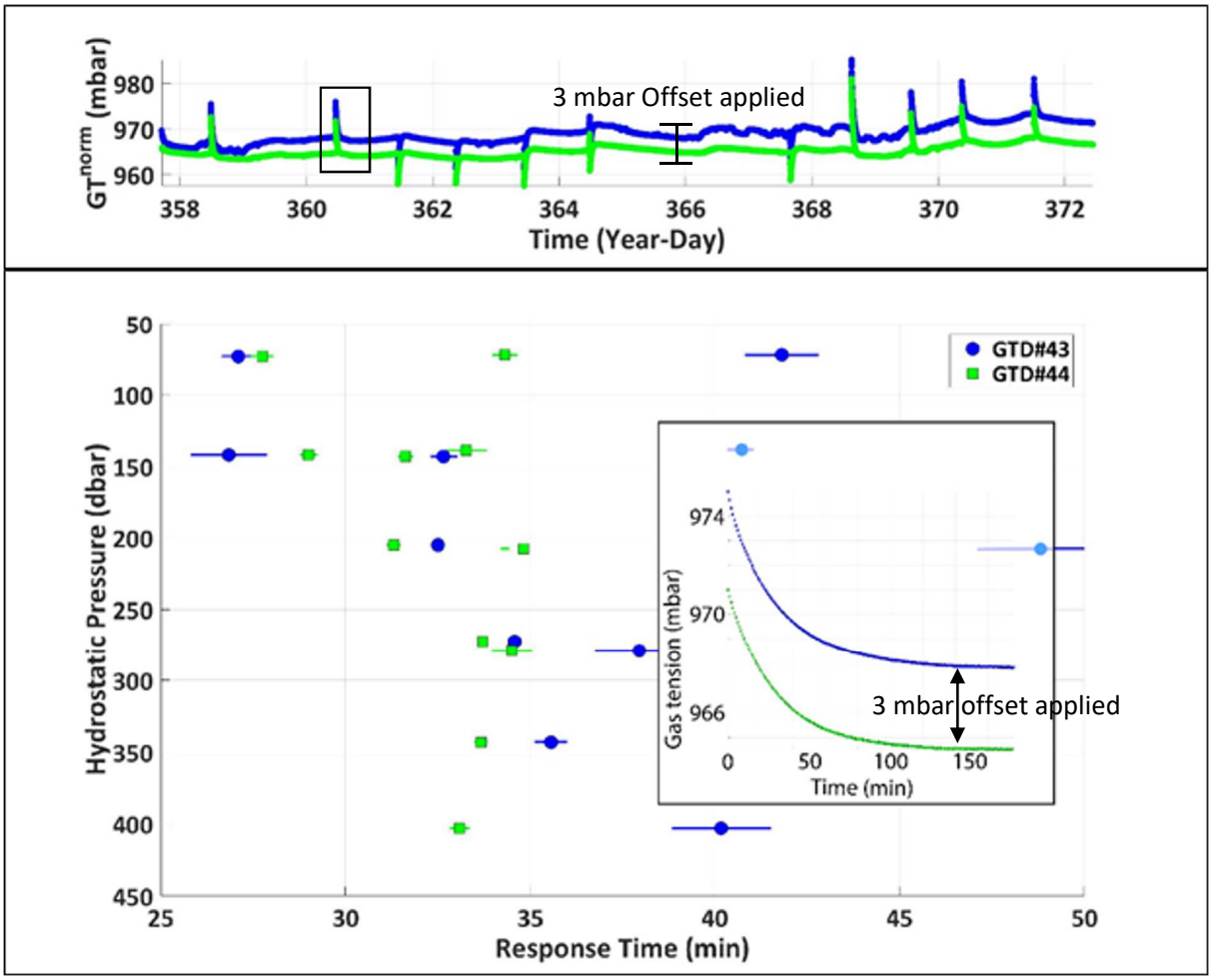

Figure 3. Results of lab experiment 1 - Top: The normalized gas tension time series corrects for the effects of temperature, hydrostatic pressure, and biology, using the best fit parameters from Table 2. Each discontinuity in the normalized gas tension time series occurs at a change in hydrostatic pressure, when the GTDs re-equilibrate. The highlighted box represents the inset below. A 3 mbar offset is applied to the GTD#44 time series to make the time series visible. Bottom: GTD#43 (blue circles) and GTD#44 (green squares) response times are independent of hydrostatic pressure, a significant advance over previous GTD versions. An individual response time is calculated by fitting a curve to a GTD equilibration (inset, curves offset by 3 mbar). Data collected with 50%-pumping. Response times for GTD#43 increased over time (print: color)

Response times for an atmospheric mixture of dissolved gases showed an inverse linear relationship with temperature (Figure 4), decreasing from 17.4 ± 1.8 min at 5.3°C to 13.0 ± 1.2 min at 29.9°C. Calculated exponential constant was 7.7 ± 2.2 kJ/mol. Literature comparisons were 4.6 (N_2) and 3.4 (O_2) kJ/mol for Teflon-AF 2400 [Alentiev et al. 2002].

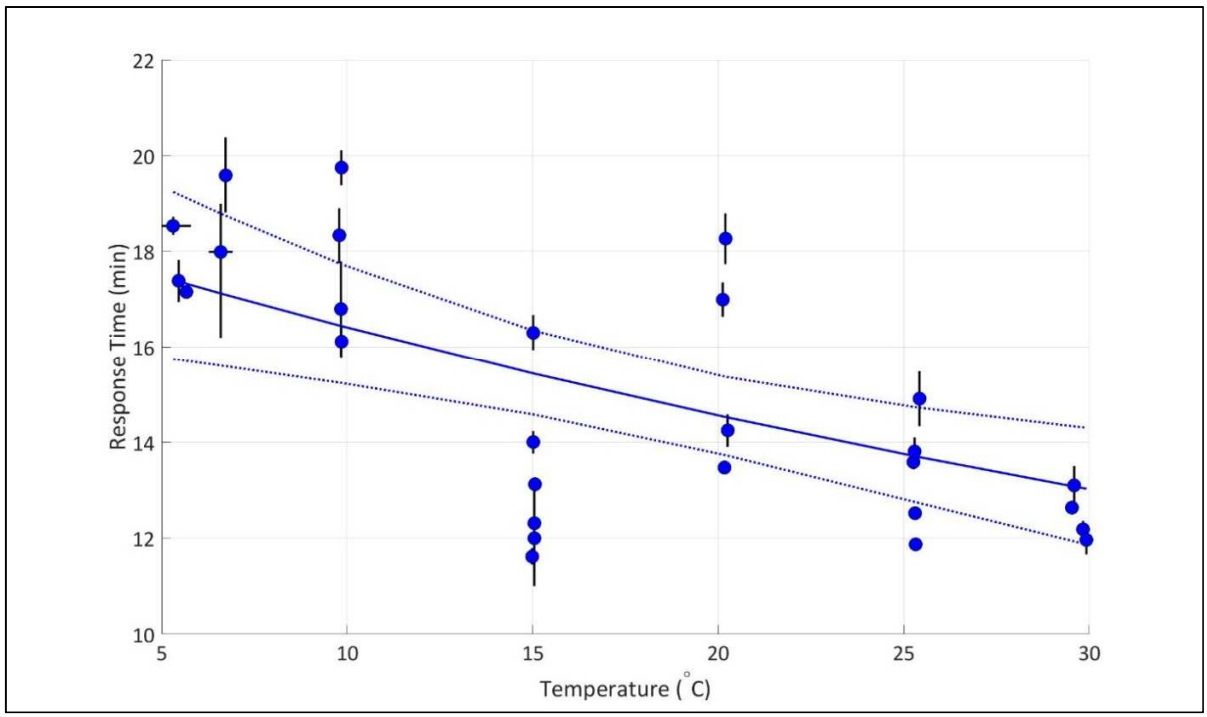

Figure 4. Results of lab experiment 2 - Continuously-pumped response times of the Teflon-membrane mounted in GTD#43 are inversely dependent on temperature. The dependence and 95% confidence intervals are fit following Equation 12. Note that the thermal response time for a pulse-pumped system will be larger.

4.2. Puget Sound

Gas tension was successfully recorded only by GTD#44 mounted on Float 77 (GTD#43 did not record properly) (Figure 5). Both GTDs successfully recorded internal temperatures. The

513 seawater temperature ranged from 10.4°C at the surface to 8.0°C at 140 dbar. Salinity varied
514 from 27.77 psu at the surface to 29.72 psu at 140 dbar. Thermal equilibration times (ϕ) were
515 21.4 ± 7.0 min and 28.2 ± 4.8 min for GTD43 and GTD44, respectively. Response times with
516 pulse-pumping (10 %) averaged τ = 36 minutes, which is still larger than the thermal response
517 time. Argon was calculated from the O_2:Ar and SBE43 oxygen concentrations. Estimated gas
518 tension agrees, to within 2 – 4 mbar (0.2% - 0.4%), with the independent IRMS N_2:Ar and O_2:Ar
519 gas tension (Figure 6).

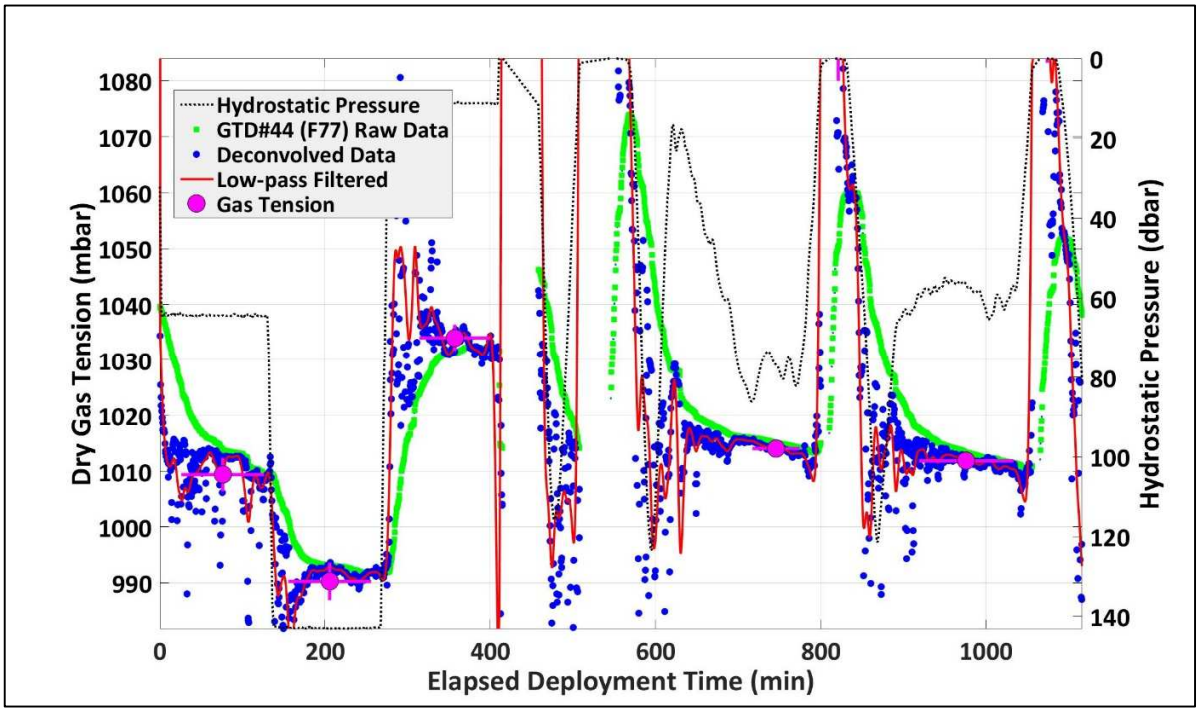

Figure 5. Successful measurements of gas tension in the Puget Sound by GTD#44 on Float 77. The procedure deriving the gas tension from the collected raw data is demonstrated. The raw data from GTD#44 on Float 77 (green squares) is deconvolved (blue circles) with a pulse-pumping response time τ = 36 minutes, and low-pass filtered (red line), which is averaged over a constant hydrostatic pressure (black lines) to arrive at the gas tension measurement (magneta circles). Floats were attached to the ship winch before the 500 minute mark and freely profiling after. (print: color)

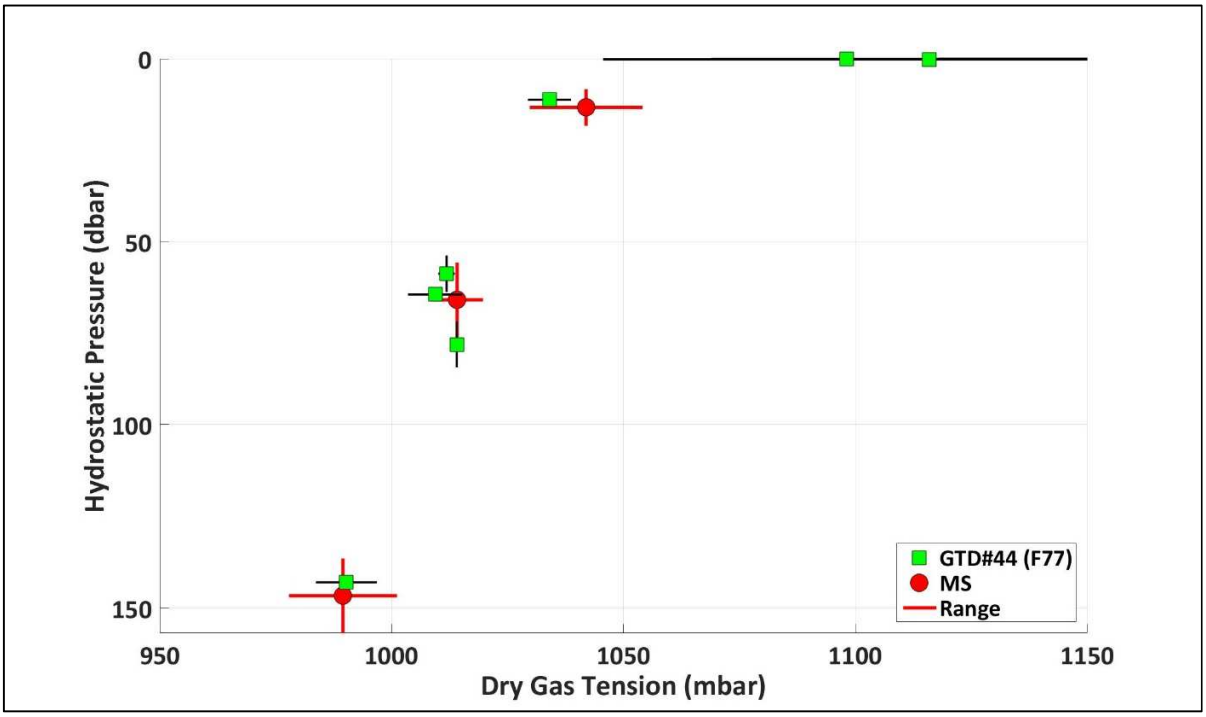

Figure 6. GTD#44 on Float 77 successfully measured gas tension throughout the water column in the Puget Sound, whether the sensor was tethered or freely drifting. The mass spectrometry (MS) data points show the target range of measured gas tension. The GTD agrees within 2 – 4 mbar (0.2 – 0.4%).

4.3. Eastern Tropical North Pacific

The oxycline, where oxygen rapidly decreases from saturation to anoxia, was located at approximately 50 – 70 dbar in the water column. Gas tension decreased from approximately atmospheric at the surface to a local minimum just below the oxycline, then a small local maximum, and then an absolute minimum of 836 mbar at 127 dbar (Figure 7). Below the absolute minimum the gas tension increases with depth. Both GTDs operated without displaying any behavior indicative of a blockage as occurred in the Puget Sound. The Argo float

542 successfully equilibrated and measured gas tension twice during separate 12-hour drifts. The
543 GTDs did not fully equilibrate at the surface due to the profiling schedule set for the floats.
544 Gas tension from Float 77 is approximately 7 mbar higher than gas tension from Float 78
545 throughout the anoxic portion of the water column without any dependence on hydrostatic
546 pressure or temperature (Figure 7). Argo float measurements are approximately 3 mbar higher
547 than the Float 77 measurements. Measured gas tension agrees to within error with the calibration
548 gas tension (Figure 8).
549

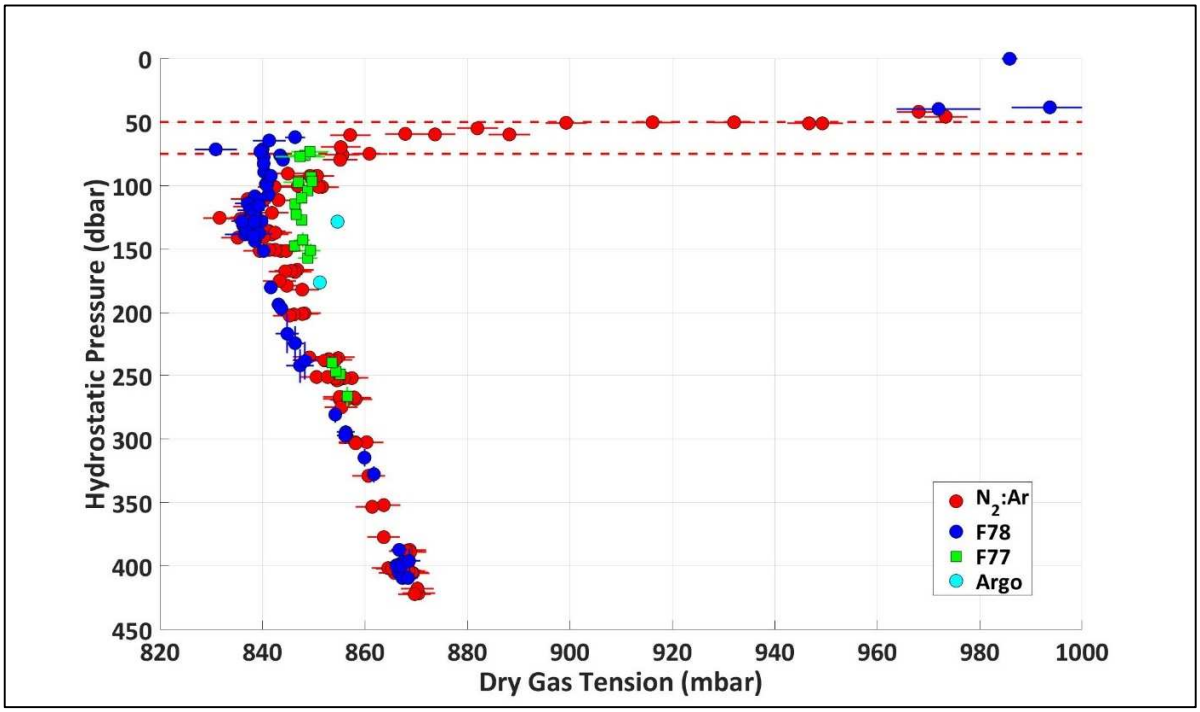

550
551 Figure 7. Gas tension within the anoxic portion of the water column was successfully measured
552 to within ±3.13 mbar of the N_2:Ar-derived validation gas tension in the ETNP ODZ. The
553 oxycline, located from approximately 50 – 70 dbar and identified with the two red lines, is where
554 the oxygen concentrations decline from saturation to sub-micromolar (< 1 µM/kg)
555 concentrations. The GTD on Float 77 measures approximately 7 mbar higher than Float 78

556 within the anoxic portion of the water column. The GTDs were pulse-pumped and floats freely-
557 drifting. The Argo float is unpumped. (print: color)

558

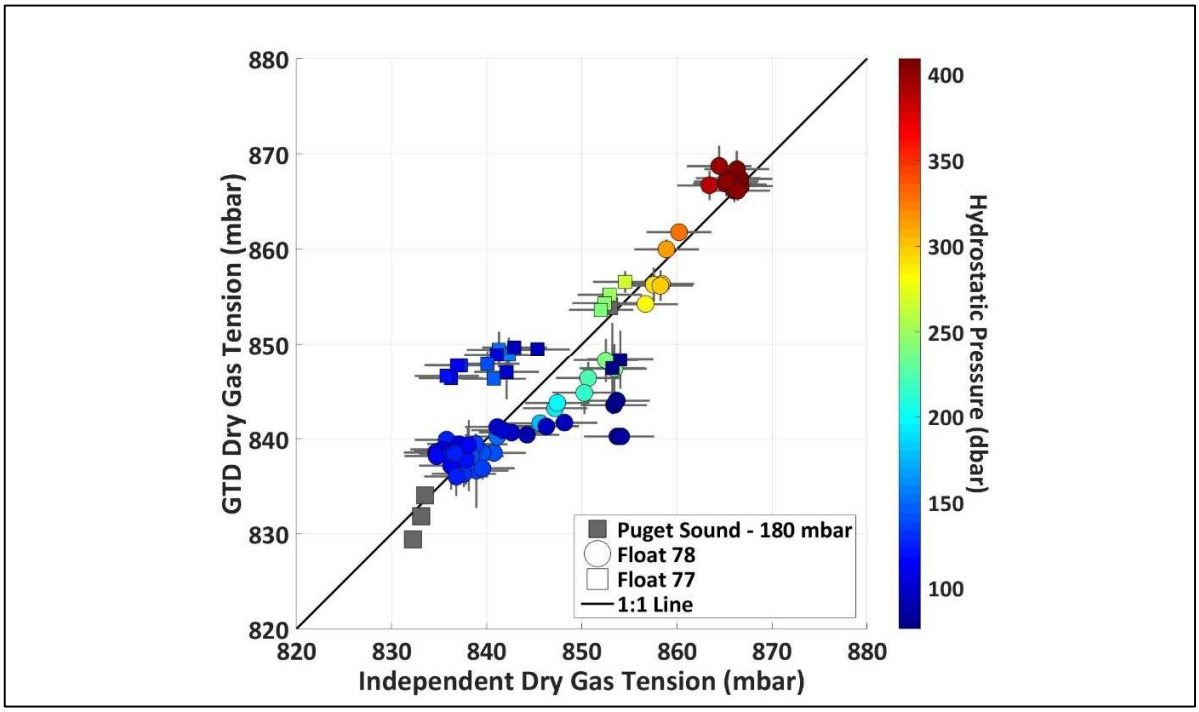

559

560 Figure 8. Validation that we successfully measured gas tension using the GTDs in the ETNP
561 ODZ. The gas tension measured by the GTD (y-axis) generally agrees within error with the
562 independent gas tension derived from the N_2:Ar measurements (x-axis). Puget Sound (grey
563 squares) are adjusted 180 mbar to fit on scale. Hydrostatic pressure of the measurements shown
564 with a linear color scale. (print: color)

565

566 **4.4. Sources of Error**

567 Changes in temperature and hydrostatic pressure not only alter the gas tension in the
568 water but may also affect how well the GTDs operate. Under the tightly controlled conditions of

569 the laboratory PTV, GTD#43 and GTD#44 measure to within ±0.2 mbar of each other. Model
570 characterization describes the GTD response to ±2.13 (GTD#43) and ±1.32 mbar (GTD#44).
571 In the Puget Sound and ETNP, uncertainty in determining the end-point equilibrated gas
572 tension is affected by the background geophysical noise. The uncertainties following
573 deconvolution and low-pass filtering, which are calculated by taking the standard deviation of
574 the low-pass filtered data for a drift following GTD equilibration, average ± 1.29 mbar (0.15%)
575 and ± 1.44 mbar (0.17%) for GTD#44 (Float 77) and GTD#43 (Float 78), respectively.
576 Geophysical noise is comprised of physical processes, such as internal waves, which alter in-situ
577 gas tension and temperature faster than the GTD can equilibrate, introducing high-frequency
578 variability. The high-frequency variability is further amplified by applying the deconvolution
579 procedure.
580 Assessment of the accuracy of the GTD gas tension is influenced by how well we can
581 independently determine the gas tension in the water column from the N_2:Ar and O_2
582 measurements. The N_2:Ar measurements themselves have a precision of 0.23‰ [Charoenpong et
583 al. 2014]. Seabird and optode oxygen errors are ≈2 µM/kg with respect to Winkler titrations.
584 However, the oxygen errors only contribute to uncertainty within the oxycline and surface; in the
585 anoxic portion of the water column, oxygen is below 100 nM and its contribution to the total
586 uncertainty is negligible [Tiano et al. 2014]. Interpolation of the argon concentrations measured
587 by Fuchsman et al [2017] has an uncertainty of 0.03 µM/kg, which with solubility uncertainty of
588 0.13% results in an average pAr uncertainty of 0.03 mbar (0.26%) [Hamme & Emerson 2004].
589 Propagation of the argon uncertainty when calculating the nitrogen concentrations from N_2:Ar is
590 the dominant source of the uncertainty in the final pN_2 of 3.15 mbar (0.31%). The total
591 uncertainty amounts to 3.42 mbar (0.40%), of which 92% is attributed to uncertainty on pN_2,

592 7.8% to pO_2, and 0.2% to pAr. The final uncertainties are 15 – 30% the size of the signal we aim
593 to resolve.

594 Final accuracy of the GTDs, assessed by comparison of the GTD gas tension with the
595 independent gas tension calculated from the N_2:Ar measurements, are 0.6% (GTD#44; Float 77)
596 and 0.4% (GTD#43; Float 78; refer to Figure 8). We take this as a conservative error estimate,
597 since at this time we cannot claim that the differences are due to a systematic bias rather than
598 random error and uncertainty.

599

600 **5. Discussion**

601 GTD#43 on Float 78 successfully measured gas tension in the ETNP ODZ to within
602 0.40%. This compares favorably with the error estimate of 0.7% on previous GTD versions
603 [McNeil et al. 1995]. The cause of the 7-mbar offset of GTD#44 relative to GTD#43 cannot yet
604 be determined. The two barometers measured to within less than 0.2 mbar difference in pre-and-
605 post cruise calibrations. Additionally, the difference between the two deployed GTDs is constant
606 throughout the water column, and shows no change with depth or temperature. However, this
607 does suggest we successfully characterized the effects of changing temperature and hydrostatic
608 pressure on the GTDs. Additionally, our final uncertainties are about 15-30% of the expected 10
609 - 20 mbar N_2 signal produced by denitrification in the ETNP, which is the primary motivation for
610 this work. Thus, these GTDs are sufficiently precise to separate a small 20 mbar signal from a
611 large 850 mbar signal.

612 Our descriptive model estimates the Henry's Law pressure dependence as 12.8 ± 0.3%
613 per 1000 dbar. This is lower than the limited literature estimates of 14% per 1000 dbar [Ludwig
614 & Macdonald 2005]. Additionally, we fit a simple linear regression of gas tension vs hydrostatic

615 pressure from the gas tension minimum to the maximum depth measured, spanning 300 dbar.
616 The fit yielded a 13.2 ± 2.8% increase per 1000 dbar. This agrees with the literature values, but
617 ignores the microbial-processes which alter gas tension in the OMZ [Klots 1961; Enns et al.
618 1964; Ludwig & Macdonald 2005].

619 The estimates of the hydrostatic pressure effect and equilibration times are complicated
620 by confounding factors not explicitly controlled. In the lab, changes in hydrostatic pressure are
621 altered using a secondary steel overflow tank with a bladder that forces water into or accepts
622 water from the main tank. The water within the secondary tank was rapidly reduced via oxidation
623 of the steel tank. Thus, changes in hydrostatic pressure create instantaneous jumps in dissolved
624 oxygen that are not readily quantifiable. Biology and rust products may also alter flow of or
625 physically coat the membrane from the water, impeding gas exchange and equilibration. This
626 complicates and introduces error to the interpretation of the hydrostatic pressure effect on gas
627 tension in the lab. It also adds variability when calculating the equilibration times from the
628 individual curve fits, because equilibration is dependent on renewal of the water-side membrane
629 boundary layer. Additionally, we suspect that these processes disproportionately affected
630 GTD#43 in the PTV over GTD#44 because GTD#43 response times increased over time. We are
631 unsure why GTD#43 was affected, but suspect its placement in the PTV relative to the overflow
632 tank and pressurization bladder was important.

633 In the ETNP ODZ, active nitrogen loss processes such as denitrification and anammox
634 actively alter the dissolved nitrogen levels [Gruber & Sarmiento 1997; Paulmier & Ruiz-Pino
635 2008; Chang et al. 2012]. Knowing the effect of hydrostatic pressure on gas solubility is
636 necessary to accurately calculate the nitrogen concentrations from the gas tension measurements.
637 Similarly, both the Anderaa Oxygen Optode and SBE43 oxygen sensor functionally measure the

partial pressure of oxygen, not the concentration [Demas et al. 1999; Carlson 2002]. Although both oxygen sensors have confounding hydrostatic pressure effects, they are calibrated to the surface solubility [Uchida et al. 2008; McNeil & D'Asaro 2014]. This led us to utilize the literature value of 14% 1000 $dbar^{-1}$ for our calculations. Consequently, we aim to further refine the hydrostatic pressure effect on gas tension by future experimentation utilizing the new GTD.

Gas tension sampling was not flawless. There was an apparent internal blockage in GTD#44 during field testing in the Puget Sound. While the source of the blockage is not yet certain, we suspect condensation of water vapor on internal piping due to rapid profiling because the floats were tethered to the ship winch. This should not be an issue when the floats profile autonomously by adjusting their buoyancy, since it results in much slower ascent and descent rates. Indeed, we observed no blockages in the ETNP. The goal is to keep the internal GTD temperature close to equilibrium with the surrounding water temperature to avoid condensation of water vapor. Additionally, membrane diffusion coefficients change by ≈28.5% over the operational temperature range of the GTD. However, the response of $\tau(T)$ is linear and is simple to adjust needed response times based on water temperature.

6. Conclusions

The new Teflon-membrane GTD offers a compact, stable method for in-situ determination of total dissolved gas pressure. It eliminates, or at the least minimizes, many of the complications of the previous PDMS-membrane version: the response time is independent of hydrostatic pressure, there is no apparent reverse-osmosis, and it functions uniformly throughout operational water depths. We demonstrate that two GTDs successfully measured to within an error of 0.4% and 0.6% the gas tension in the ETNP ODZ. Additionally, we showed that a GTD

661 can equilibrate and measure gas tension on an Argo-float. Using previously published methods
662 for determining dissolved nitrogen from measured gas tension, the new GTD opens up the
663 possibility for in-situ investigation of denitrification within pelagic ODZs [McNeil et al. 2005;
664 McNeil et al. 2006a]. An additional advantage to this version of the float-mounted GTD is it is
665 significantly more compact than the previous PDMS-version. Further reduction in response time
666 should be possible using a pressure sensor with a very small internal volume. A faster response
667 time should also reduce the uncertainty due to geophysical noise.

668 We envision a variety of future applications for our new GTD. Its compact size and low-
669 power makes it an ideal candidate to be incorporated onto biogeochemical-Argo-floats for long
670 term in-situ studies of denitrification in ODZs, air-sea gas exchange, and net community
671 production in the surface ocean. Continuing improvements in shrinking the size and response
672 time are also targeted at future incorporation onto CTDs as part of the standard instrument
673 package. Our goal is to make gas tension measurements and dissolved-N_2 gas a regularly
674 collected parameter, alongside T, S, and O_2.

675

676

677

678

679

680

681 **Acknowledgements**

682 The authors would like to thank the Captain and crew of the *R/V New Horizon*, Co-Chief
683 Scientist Frank Stewart for providing ship space, Happy Hu for Winkler collection and sampling,

684 and Anne Cruz for sample collection, and Clara Fuchsman for sharing her argon concentration
685 profiles from the ETNP. We would also like to thank the reviewers of our manuscript for the
686 helpful comments and suggestions during revisions.
687
688 **Funding:** This work was supported by the National Science Foundation Grant numbers 1153295
689 (McNeil & D'Asaro) and 1154741 (Altabet).
690
691 **COI Statement:** B. Johnson and C. McNeil disclose significant financial interests as they are
692 president and vice president, respectively, of Pro-Oceanus Systems, Inc. (Bridgewater, NS,
693 Canada). Pro-Oceanus is the manufacturer of the GTDs used in this study.
694
695
696
697
698
699
700
701
702
703
704 **References**

1. Alentiev, A.Y., Shantarovich, V.P., Merkel, T.C., Bondar, V.I., Freeman, B.D., Yampolskii, Y.P. 2002. Gas and Vapor Sorption, Permeation, and Diffusion in Glassy Amorphous Teflon AF1600. *Macromol. 35, 9513-9522.* DOI:10.1021/ma020494f
2. Bernardo, P., Drioli, E., Golemme, G. 2009. Membrane Gas Separation: A Review/State of the Art. *Ind. Eng. Chem. Res. 48, 4638-4663.* DOI:10.1021/ie8019032
3. Boyer, T.P., Antonov, J.I., Baranova, O.K., Coleman, C., Garcia, H.E., Grodsky, A., Johnson, D.R., Locarnini, R.A., Mishonov, A.V., O'Brien, T.D., Paver, C.R., Reagan, J.R., Seidov, D., Smolyar, I.V., Zweng, M.M. 2013. World Ocean Database 2013, NOAA Atlas NESDIS 72, S. Levitus, Ed., A. Mishonov, Technical Ed.; Silver Spring, MD, 209 pp., DOI:10.7289/V5NZ85MT
4. Bragg, H.M., Johnston, M.W. 2016. Total dissolved gas and water temperature in the lower Columbia River, Oregon and Washington, water year 2015. U.S. Geological Survey Open-File Report 2015-1212, 26p., DOI:10.3133/ofr20151212
5. Carlson, J. 2002. Development of an Optimized Dissolved Oxygen Sensor for Oceanographic Profiling. *International Ocean Systems 6(5), 20-21*
6. Chang, B.X., Devol, A.H., Emerson, S.R. 2012. Fixed nitrogen loss from the eastern tropical North Pacific and Arabian Sea oxygen deficient zones determined from measurements of N_2:Ar. *Global Biogeochem. Cycles 26(3), GB3030.* DOI
7. Charoenpong, C., Bristow, L.A., Altabet, M.A. 2014. A continuous flow isotope ratio mass spectrometry method for high precision determination of dissolved gas ratios and isotopic composition. *Limnol. Oceanogr. Methods 12, 323-337.* DOI:

8. D'Asaro, E., McNeil, C.M. 2007. Air-sea gas exchange at extreme wind speeds measured by autonomous oceanographic floats. *J. Mar. Syst. 66, 92-109.* DOI:10.1016/j.jmarsys.2006.06.007
9. D'Aoust, B.G., White, R., Seibold, H. 1975. Direct measurement of total dissolved gas pressure. *Undersea Biomedical Research 2(2), 141-149*
10. Demas, J.N., DeGraff, B.A., Coleman, P.B. 1999. Oxygen Sensors based on luminescence quenching. *Anal. Chem. 71, 793A-800A*.
11. Emerson, S., Bushinsky, S. 2016. The role of bubbles during air-sea gas exchange. *J. Geophys. Res. Oceans 121, 4360-4376.* DOI:10.1002/2016JC011744
12. Enns, T., Scholander, P.F., Bradstreet, E.D. 1964. Effect of Hydrostatic Pressure on Gases Dissolved in Water. *J. Phys. Chem. 69(2), 389-391*
13. Fickeisen, D.H., Schneider, M.J., Montgomery, J.C. 1975. A Comparative Evaluation of the Weiss Saturometer. *Trans. American Fisheries Soc. 104(4), 816-820*
14. Fuchsman, C.A., Devol, A.H., Casciotti, K.L., Buchwald, C., Chang, B.X., Horak, R.E.A. 2017. An N isotopic mass balance of the Eastern Tropical North Pacific oxygen deficient zone. *DSR II: Topical Studies in Oceanography*, doi:10.1016/j.dsr2.2017.12.013
15. Groffman, P.M., Altabet, M.A., Böhlke, J.K., Butterback-Bahl, K., David, M.B., Firestone, M.K., Giblin, A.E., Kana, T.M., Nielsen, L.P., Voytek, M.A. 2006. Methods for Measuring Denitrification: Diverse Approaches to a Difficult Problem. *Ecol. Appl. 16(6), 2091-2122.* DOI: 10.1890/1051-0761(2006)016[2091:MFMDDA]2.0.CO;2
16. Gruber, N., Sarmiento, J.L. 1997. Global patterns of marine nitrogen fixation and denitrification. *Global Biogeochem. Cycles 11(2), 235-266.* DOI:

17. Hales, B., Chipman, D., Takahashi, T. 2004. High-frequency measurement of partial pressure and total concentration of carbon dioxide in seawater using microporous hydrophobic membrane contactors. *Limnol. Oceaongr. Methods 2, 356-364.*

18. Hamme, R.C., Emerson, S.R. 2004. The solubility of neon, nitrogen, and argon in distilled water and seawater. *Deep-Sea Res. I 51, 1517-1528.* doi:10.1016/j.dsr.2004.06.009

19. Hamme, R.C., Emerson, S.R. 2004b. Measurement of dissolved neon by isotope dilution using a quadrupole mas spectrometer. *Mar. Chem. 91*, *53-64*. doi:10.1016/j.marchem.2004.05.001

20. Hamme, R.C., Berry, J.E., Klymak, J.M., Denman, K.L. 2015. In situ O_2 and N_2 measurements detect deep-water renewal dynamics in seasonally-anoxic Saanich Inlet. *Cont. Shelf Res. 106, 107-117.* doi:10.1016/j.csr.2015.06.012

21. Kennish, M.J. (editor) (1989) *Practical Handbook of Marine Science*. C.R.C. Press, Inc., Boca Raton, Florida, 710 pp.

22. Klots, C.E. 1961. Effect of Hydrostatic Pressure upon the solubility of gases. *Limnol. Oceaongr. 6(3), 365-366.* doi:10.4319/lo.l1961.6.3.0365

23. Lagarias, J.C., Reeds, J.A., Wright, M.H., Wright, P.E. 1998. Convergence Properties of the Nelder-Mead Simplex Method in Low Dimensions. *SIAM J. of Optim. 9(1), 112-147.* doi:10.1137/S1052623496303470

24. Langdon, C. 2010. Determination of dissolved oxygen in seawater by Winkler titration using the amperometric technique. *The GOSHIP Repeat Hydrography Manual: a Collection of Expert Reports and Guidelines, edited by: Hood, EM, Sabine, CL, and Sloyan, BM.*

769 25. Löffler, A., Schneider, B., Schmidt, M., Nausch, G. 2011. Estimation of denitrification in
770 Baltic Sea deep water from gas tension measurements. *Marine Chemistry 125, 91-100*.
771 doi:10.1016/j.marchem.2011.02.006
772 26. Ludwig, H., Macdonald, A.G. 2005. The significance of the activity of dissolved oxygen, and
773 other gases, enhanced by high hydrostatic pressure. *Comp. Biochem. Physiol. Part A 140,*
774 *387-395.* doi:10.1016/j.cbpb.2005.02.001
775 27. Manning, A.H., Solomon, D.K., Sheldon, A.L. 2003. Application of a total dissolved gas
776 pressure probe in ground water studies. *Ground Water 41(4): 440-448*. DOI:10.1111/j.1745-
777 6584.2003.tb02378.x
778 28. McNeil, C.L., Johnson, B.D., Farmer, D.M. 1995. *In-situ* measurement of dissolved nitrogen
779 and oxygen in the ocean. *Deep-Sea Res. I 42(5), 819-826.* DOI:10.1016/0967-
780 0637(95)97829-W
781 29. McNeil, C., Katz, D., Wanninkhof, R., Johnson, B. 2005. Continuous shipboard sampling of
782 gas tension, oxygen, and nitrogen. *Deep-Sea Res. I 52, 1767-1785.*
783 doi:10.1016/j.dsr.2005.04.003
784 30. McNeil, C., D'Asaro, E., Johnson, B., Horn, M. 2006a. A Gas Tension Device with
785 Response Times of Minutes. *J. Atmos. Oceanic Tech. 23, 1539-1558.*
786 doi:10.1175/JTECH1974.1
787 31. McNeil, C.L., D.R. Katz, B. Ward, W.R. McGillis, and B.D. Johnson. 2006b. A method to
788 estimate net community metabolism from profiles of dissolved O_2 and N_2. *Hydrobiologia*
789 *571:181-190.* DOI:10.1007/s10750-006-0236-7
790 32. McNeil, C.L., and E.A. D'Asaro. 2007. Parameterization of air-sea gas fluxes at extreme
791 wind speeds. *J. Mar. Syst. 66, 110-121.* doi:10.1016/j.jmarsys.2006.05.013

792 33. McNeil, C.L, D'Asaro, E.A. 2014. A calibration equation for oxygen optodes based on
793 physical properties of the sensing foil. *Limnol. Oceanogr. Methods, 12, 139-154.*
794 doi:10.4319/lom.2014.12.139
795 34. Paulmier, A., Ruiz-Pino, D. 2008. Oxygen minimum zone (OMZs) in the modern ocean.
796 *Prog. Oceanogr. 80, 113-128.* doi:10.1016/j.pocean.2008.08.001
797 35. Pinnau, I., Toy, L.G. 1996. Gas and vapor transport properties of amorphous perfluorinated
798 copolymer membranes based on 2,2-bistrifluoromethlyl-4,5-difluoro-1,3-
799 diioxole/tetrafluoroethylene. *J. Membr. Sci. 109, 125-133.* doi:10.1016/0376-7388(95)00193-
800 X
801 36. Takahashi, T., Feely, R.A., Weiss, R.F., Wanninkhof, R.H., Chipman, D.W., Sutherland,
802 S.C., Takahashi, T.T. 1997. Global air-sea flux of CO_2: An estimate based on measurements
803 of sea-air pCO_2 difference. *PNAS 94(16), 8292-8299.*
804 37. Tiano, L., Garcia-Robledo, E., Dalsgaard, T., Devol, A.H., Ward, B.B., Ulloa, O., Canfield,
805 D.E., Revsbech, N.P. 2014. Oxygen distribution and aerobic respiration in the north and
806 south eastern tropical Pacific oxygen minimum zones. *Deep-Sea Res. I 94, 173-183.*
807 doi:10.1016/j.dsr.2014.10.001
808 38. Uchida, H., Kawano, T., Kaneko, I., Fukasawa, M. 2008. In Situ Calibration of Optode-
809 Based Oxygen Sensors. *J. Atmos. Oceanic Techn. 25, 2271-2281.*
810 doi:10.1175/2008JTECHO549.1
811
812